Received: 30 April 2021 | Revised: 17 June 2021 | Accepted: 6 July 2021

DOI: 10.1002/pc.26216

RESEARCH ARTICLE

Polymer COMPOSITES WILEY

Investigation of nonisothermal fusion bonding for extrusion additive manufacturing of large structural parts

Nevine Tagscherer[1,2] | **Patrick Consul**[1] | **Ingo Leonard Kottenstedde**[2,3] | **Houyem Latiri**[1] | **Swen Zaremba**[1] | **Klaus Drechsler**[1]

[1]TUM Department of Mechanical Engineering, Chair of Carbon Composites, Technical University of Munich, Garching bei München, Germany

[2]Research, New Technologies, Innovations, BMW Group, Munich, Germany

[3]Department of Chemistry, University of Paderborn, Paderborn, Germany

Correspondence
Nevine Tagscherer, BMW Group, Research, New Technologies, Innovations, Petuelring 130, 80788 Munich, Germany.
Email: nevine.tagscherer@bmwgroup.com

Abstract

Fusion bonding is understood to be the decisive mechanism for the interlayer strength in extrusion additive manufacturing. This study links the characteristic temperatures of semicrystalline thermoplastics, namely, PA6 with 40% carbon fibers, to the bond formation in respect to real-world processing conditions. Based on theoretical investigations, a process window is proposed for bonding to occur without polymer degradation. This range from the glass transition to the initial degradation temperature was determined through differential scanning calorimetry and thermogravimetric analysis. A second process window for optimal bonding is proposed from the extrapolated onset crystallization temperature, T_{eic}, to the melt temperature, T_m. The validation of these process windows was conducted by bending tests according to DIN EN 178. T_m was confirmed as the upper limit, with the part's geometric integrity compromised at higher temperatures. T_{eic} had to be refuted as lower limit as no discrete reduction in bond strength was determined in alignment with T_{eic}. Authors suggest the lower limit is defined by the lowest substrate temperature to lead to interface temperatures above the onset of melt temperature. By utilizing thermal analyses, less time and resources are required to detemine a suitable process window for extrusion additive manufacturing.

KEYWORDS

3D printing, adhesion, carbon fibers, extrusion, thermal analysis, thermal properties

1 | INTRODUCTION

Additive manufacturing (AM) has become integral to the manufacturing world, and its versatility has enabled it to enter new markets.[1] Compared to traditional subtractive methods, AM facilitates small batch production with a high degree of individualization.[2,3] Low scrap rates make it attractive for applications involving high-cost materials, while its geometric flexibility and large potential for digitalization and automation have advanced the use of additive manufacturing from mere prototyping to small serial productions.[3]

In recent years, various AM technologies, particularly material-extrusion-based AM, have progressed and increased in their applications.[4,5] This paper focuses on extrusion additive manufacturing (EAM), which contrary to

fused filament fabrication (FFF), uses pelletized feedstocks instead of filaments. This enables material cost reductions, as well as higher deposition rates.[6] Multiple studies have demonstrated the potential of generally increasing the throughput and printing speeds of FFF and EAM to tailor larger, more efficient and cost-effective AM processes.[1,6–8]

One of the greatest challenges of extrusion-based processes in industrial scale applications is the directional bias of the mechanical properties in the build direction.[6,9,10] This is mostly the result of both insufficient fusion bonding of consecutive layers due to nontailored temperature conditions and macro porosity, created by the rounded bead geometry. Incomplete fusion bonding in turn reduces the mechanical properties in comparison to the bulk material.[6,11]

To achieve bulk-like mechanical properties in all directions of the part, interlayer bonding must be optimized. For basic thermal and bonding models for EAM, analogies can be drawn from injection molding, thermoplastic welding, and tape laying.[12] In injection molding, the temperatures of the melt and mold have the most significant effect on the final part's properties.[13] Similarly, the weldline properties of welded semicrystalline thermoplastics approach those of the bulk material for processing temperatures around the melting point.[14]

Compared to thermosets, thermoplastics melt due to their lack of crosslinks. Furthermore, they offer distinct advantages such as improvements of several mechanical and chemical properties, recyclability and reparability, low costs, and shorter cycle times.[15–17] Based on these advantages, they are increasingly being used in the automotive and general transport sector.[18] In additive manufacturing, thermoplastics challenge AM processes by virtue of their high viscosities, as they require high temperatures and pressures to initiate polymer flow during extrusion.[19,20]

Semicrystalline polymers make up a considerable proportion of thermoplastics used in AM. Their morphological structure leads to a high dependency on mechanical properties on the processing conditions and the resulting degree of crystallization.[17,18,21] Processing temperatures above the melting point reduce the viscosity and mobilize molecules for polymer flow.[12] Polyamide 6 (nylon 6) is well suited for high heat and stress resistance applications and thus has become a common engineering polymer used in the automotive industry, for instance, in injection molding processes.[22] Its crystalline structure promotes a glass transition between 45 and 80°C, and melting at around 230°C.[23,24]

Insufficient polymer properties can be overcome by the addition of fiber reinforcements.[25,26] While this can increase a part's stiffness by three to seven times,[6,27] the use of recycled short fibers from production scrap is a step toward waste-reduced production. Furthermore, the transition from continuous fibers to short fibers enables pellet processing, directly increasing cost effectiveness, while still providing increased stiffness and strength.[3,6]

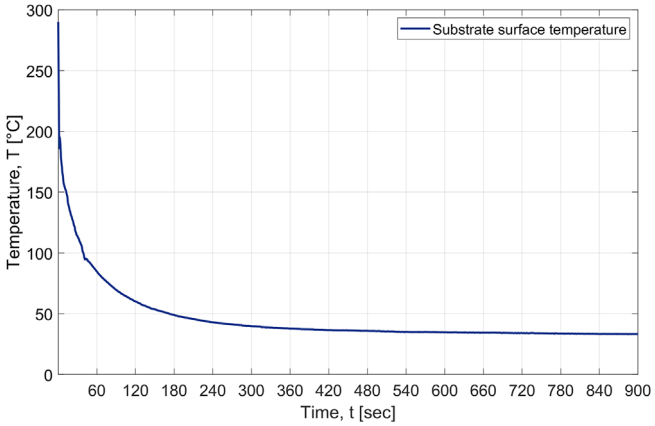

FIGURE 1 Cooling curve of the substrate surface temperature of PA6 CF40 after bead deposition

The intended operational system is a robot-based EAM facility fed with short-carbon-fiber-reinforced PA6 pellets and the ability to produce thin-walled parts up to $4 \times 2 \times 2$ m. Figure 1 shows the time-dependent cooling curve, which makes it clear that the substrate temperature drops rapidly below the glass transition. This creates the need for external substrate heating in order to optimize bonding even for large parts.[11,28]

Researchers have defined process windows for improved fusion bonding of AM feedstocks based on thermal analyses, while only considering the glass transition and decomposition of the material.[29] Many times, processing parameters have also been optimized solely by mechanical testing of the part's bond strength. This paper, therefore, strives to link the thermal properties of thermoplastics to their fusion bonding ability to allow a more effective and process-tailored mechanical testing.

The effect of thermal properties of thermoplastics, specifically short-carbon-fiber-reinforced polyamide 6, on their fusion bonding capabilities during layer-wise additive manufacturing is considered by means of a theoretical investigation. A comprehensive thermal analysis is presented to explain the impact of processing conditions on the investigated properties and to define a process-tailored processing window. A suggestion is provided for validation of the results in terms of mechanical bond strength, though its execution is still subject to further research.

2 | THEORETICAL INVESTIGATION

The optimization of fusion bonding in additive processes requires an understanding of material behavior in terms

of thermal phase changes, bond formation, and crystalline structure. Research has shown that crystallization can hinder the molecular diffusion at the layer interface.[15,17] Therefore, it must be considered to occur simultaneously with bond formation, which can lead to poor bonding and reduced mechanical properties. As part properties can also be impacted by the effects of polymer degradation, models describing degradation effects are also considered.

Fusion bonding, in terms of intimate contact and autohesion, as well as crystallization and degradation processes are strongly temperature- and time dependent.[30] These characteristic temperature ranges have to be identified in order to control the substrate and thus the interface temperature for complete fusion bonding. The general process window is limited by the minimum and maximum temperatures, between which fusion bonding can occur. A more defined process window is outlined for maximum fusion bonding and tailored specifically to the applicable EAM system.

2.1 | Fusion bonding

For the understanding of semicrystalline polymers, heat transfer, resin flow, and wetting have to be considered in addition to the bonding-rate-controlled chain diffusion.[17,20,31] As the aim of fusion bonding is to achieve a monolithic material with the strength of the bulk polymer,[20,32] the degree of bonding, D_b, describes the interlaminar bond strength of identical polymer surfaces that are in contact compared to the strength of the bulk.[17,18] The degree of bonding is calculated from the degree of intimate contact, D_{ic}, and the degree of healing, D_h:[32]

$$D_b = D_{ic}(0)\cdot D_h(t) + \int_0^t D_h(t-t')\cdot\frac{D_{ic}(t')}{dt}\,dt' \qquad (1)$$

A low D_b results from the hindered bond formation by nonideal processing conditions, which create anisotropy through regions of reduced molecular entanglement[9,11,13,25] and possible void formation, acting as initiators of crack propagation.[9,20,33] Various studies on mechanical testing of interlayer bonding showed that the interface temperature, T_{int}, is the primary factor determining the degree of bonding. Good bond formation is observed for T_{int} above the melting temperature, T_m.[18,34,35] With the constant extrusion temperature greatly exceeding T_m, the substrate temperature can be below T_m as long as the resulting T_{int} rises above T_m.[31]

Multiple models of interlaminar bond strength have been devised in an attempt to model this behavior. Dara and Loos[36] assumed that only neat resin resides at the surfaces and first defined bonding as two processes, namely, intimate contact and autohesion. Intimate contact describes a process of surface rearrangement that achieves full contact between the bonding partners, while autohesion is the phase of molecular diffusion across the interface. Lee and Springer[37] built on this with their own models of intimate contact and autohesion. Over the years, the models were extended by time and molecular scaling factors,[38] and to do justice to residual stresses and strains,[39] to consider nonisothermal conditions, varying pressures, crystallinity, and thermal degradation.[20] For fiber placement, void formation during bonding was modeled with basic assumptions of heat input and ideal heat transmission,[40] and was later expanded to nonisothermal fusion bonding.[12] Assumptions for intimate contact and autohesion will be analyzed in more detail, as a basic understanding is crucial for the definition of the process window.

2.2 | Intimate contact

When polymer surfaces are placed in contact, their microasperities and surface roughness result in a small initial area of contact.[20,25,32] As the temperature rises above the glass transition, T_g, the asperities flow into the free spaces, increasing the degree of intimate contact, D_{ic}.[16–18,25] Compared to the temperature in nonisothermal bonding, the system pressure has little effect, as the highly molten outer surface layers form nearly instantaneous contact under sufficiently high temperatures.[41]

The intrinsic features of the surface asperities and their change over time are difficult to model mathematically as they are of high geometric complexity.[42,43] Dara and Loos[36] first modeled the surface as a function of differently sized rectangular units. Lee and Springer[37] simplified this model to rectangular elements of the same size and verified it for semicrystalline polymers. As the most widely used model,[25] it describes D_{ic} as:

$$D_{ic} = \frac{1}{1+\frac{\omega_0}{b_0}}\left[1+\frac{5P_{app}}{\mu_{mf}}\left(1+\frac{\omega_0}{b_0}\right)\left(\frac{a_0}{b_0}\right)^2 t\right]^{1/5} \qquad (2)$$

where P_{app} is the applied gauge pressure, μ_{mf} is the matrix fiber viscosity and a_0, b_0, ω_0 are theoretical geometrical constraints that cannot be identified by experiment.[37,43] Yang and Pitchumani[42,43] compensated for this by accounting for the measurable asperities by way of a cantor set fractal model, for which the geometrical parameters could be identified by experiment. At the same time, the Lee and Springer model was adapted in different ways for time-varying non isothermal

conditions[20,39] and was simplified by Sonmez and Hahn[20] to:

$$D_{ic} = a^* \left[\int_0^{t_b} \frac{P_{app}}{\mu_{mf}} dt \right]^{1/5} \quad (3)$$

which can be fitted into experimental data using the constant a^*.[20] Once intimate contact is established at a point on the surface, autohesion can proceed.[44]

However, with AM, intimate contact is only established for the material residing directly under the nozzle, as no pressure except the weight of the extrudate acts on the interface after the nozzle has moved on. As this time frame for the chosen nozzle is between 0.075 and 0.013 s for slow and fast traversing speeds, the assumption of intimate contact occurring instantaneously is made.[45] Therefore, the degree of intimate contact can be reduced to

$$D_{ic}(0) = 1 - V_{Void} \quad (4)$$

where V_{Void} is the volume fraction of voids at the polymer interface. With the assumption of no in intimate contact over time: $\dot{D}_{ic}(t) = 0$.

2.3 | Autohesion

Autohesion, which is often referred to as chain, molecular or self-diffusion, healing, or autohesive strength development, is the central process when it comes to the strength formation.[44] Once intimate contact has been realized and the process has been sufficiently thermally activated, the molecular chains diffuse across the interface.[16–18] Models of autohesion are based on the reptation theory proposed by De Gennes,[46] which models the interdiffusion of amorphous polymers under isothermal conditions following intimate contact. Entangled random coil chains move through their imaginary tube of length L under the influence of Brownian motion. The reptation time, t_R is the time required for the chain to fully exit its tube for which $l/L = (t/t_R)^{1/2}$ has been found to be true.[12] t_R can be determined from experimental data by fitting the Arrhenius equation[12,47] or by frequency sweeps in parallel plate rheometry, determining the required weld time t_w as $t_w \geq t_R$.[48] Just as high temperatures lead to increased chain mobility and a shorter reptation time, low molecular masses correspond to lower viscosities due to the shorter chains and shorten the reptation time according to $t_R = M^3$.[24,38,46]

Based on De Gennes, Yang and Pitchumani[12] derived the degree of healing, D_h, for isothermal processes and later adapted their model for nonisothermal conditions to:

$$D_h = \left(\frac{l}{L_w} \right)^{1/2} = [2f(t)]^{1/4} = \left[\int_0^t \frac{1}{t_w(T)} dt \right]^{1/4} \quad (5)$$

which simplifies to:

$$D_h = \left(\frac{t}{t_R} \right)^{1/4} \quad (6)$$

The different models, with their particular advantages and disadvantages, can be used to describe crack healing at the polymer-polymer interface,[44] as well as bond formation during welding,[48] tape placement[20] and additive manufacturing. Various studies have found that the temperature of the interface must be close to or above T_m to promote fast chain diffusion. As the healing temperature increases, the diffusion rate also increases, and thus the time taken for healing decreases.[35] When healed under ideal conditions for a sufficient amount of time, the interface becomes indistinguishable from the bulk polymer.[17,19,20] Under these conditions, crystallization is a competing mechanism with autohesion and is an important phenomenon to consider.[17]

2.4 | Crystallization

During cooling and annealing, crystallization is driven by the temperature difference between the crystallization temperature, T_{pc}, and T_m, with small differences leading to slow crystal growth.[17] T_{pc} lies between T_g and T_m, where the chains are slightly mobile without melt flow occurring. A polymer kept long enough within the right temperature range rearranges its chains to form compact structures, known as crystallites.[17] These can hinder chain reptation and the molecular diffusion required for a high degree of autohesion and bulk-like properties.[15,17] Thus, the degree of crystallization and the crystal morphology determine a part's mechanical and physical properties.[20,49]

The phases of crystallization are driven by multiple factors, including molecular weight, temperature, cooling rate, pressure, orientation, flow field, and residence time at melt temperature.[13,50] The crystal growth in isothermal fusion bonding can be described on a macroscopic scale by the Avrami equation.[50,51] It has been adapted for nonisothermal processes for the interrelation of temperature and crystallization[51] as the Ozawa equation.[52]

Due to a mutual coupling of temperature and crystal growth, higher cooling rates lead to lower crystallization temperatures and a lower degree of crystallinity with smaller crystals,[51] leading to a lower transverse elastic modulus and an increase in interlaminar fracture toughness.[13,18] In semicrystalline polymers, the molecular chains align locally when heated above T_g. Once their melting point is exceeded, strong chain motion eradicates any local alignment, and the melt is present in an amorphous state.[15] The amorphous and crystalline regions of neat polyamide 6 display dissimilar mechanical properties.[53] The α-phase is formed either at isothermal temperatures above 150°C[54] −190°C[53] or through slow cooling and is thermodynamically most stable.[55] The metastable γ-phase is formed at lower crystallization temperatures or through fast cooling (10–50 K/s),[54] and can be turned into an α-phase by annealing.[53] Studies on PA6 revealed that at cooling rates above 100–150 K/s, no crystallization takes place and fully amorphous PA6 is obtained.[53,54] More details on the crystallization behavior of PA6 can be found in the literature.[21,49,56–58]

As fibers act as nucleation sites and increase the nucleation density,[25] the addition of fibers to PA6 causes a thin transcrystalline γ-layer that covers the bulk dominated by the α-phase and grows with increasing fiber volume contents (FVC), while increasing the crystallization rate.[53,59,60] Higher cooling rates serve to reduce the transcrystallinity. With research on the effects of transcrystallinity on the mechanical properties of thermoplastics is as yet indecisive, it is not considered in this study.[59]

Many thermal models and process window definitions for similar welding processes, for example, tape laying, have neglected the effect of crystallinity on bond formation.[20] However, the strong coupling between crystallite presence and chain mobility suggests that interdiffusion is hindered as crystallinity increases. A few studies have addressed this with specific reference to polyamides.[61,62]

2.5 | Polymer degradation

The thermal influence on degradation kinetics of non-isothermal processes can be measured by non-isothermal assessment through thermogravimetric analysis (TGA).[20] This prediction is based on either model-free or model-based isoconversional methods,[63] assuming that the process rate is a function of temperature and conversion $d\alpha/dt = \phi(T,\alpha)$ and that activation parameters are assessed through different isothermal measurements or sets of different heating rates.[63] Model-based methods are adapted from the degradation kinetic equations and chemical reactions occurring during degradation. Model-free methods, however, enable the determination of degradation behavior and activation energy without the knowledge of the exact kinetic equations of the material.[64] Model-free methods are based on two assumptions: (i) that degradation can be described by a single kinetic equation that specifies the degree of conversion, α:

$$d\alpha/dt = A(\alpha)f(\alpha)exp(-E(\alpha)/RT) \quad (7)$$

with activation energy $E(\alpha)$ and pre-exponential factor $A(\alpha)$; and (ii) that the change in reaction for each degree of conversion depends only on the temperature.[64,65]

Moukinha[64] suggests using model-free analyses to obtain a satisfactory decomposition model for either separated-step or single-step processes. The widely accepted Friedman method[66,67] investigates degradation kinetics at heating rates not achievable in TGA measurements, as presented in additive manufacturing. It is based on a set of multiple linear heating rates and derives a semi-empirical rate law to predict degradation behavior. The model presents a plot of $log(d\alpha/dt)$ over 1000/T, with isoconversional lines plotted. The activation energy $E(\alpha)$ can be determined from their slope.[68]

2.6 | Definition of a process window

The hypothesis of this paper is that a process window for optimized fusion bonding can be defined based on the material characteristics of the polymer. As is it easiest measured by optical sensors during any printing process, the surface substrate temperature, T_{sub}, is chosen as the temperature for defining the process window. Researchers already defined a broad processing window, in which bonding can generally occur, between the glass transition and the degradation.[29] Within this large temperature range, crystallization is presumed to hinder interdiffusion, and high temperatures lead to polymer flow and risk the part's geometric integrity. Therefore, this paper aims to tailor a narrower process window for fusion bonding optimization.

2.6.1 | Broad process window

I. Upper limit: Degradation and the decline of mechanical properties can be analyzed by thermogravimetric analysis (TGA).[65,69] DIN 51006[70] and ASTM E2550[71] define the temperature of the first deflection from the baseline as T_{ini} and T_{onset}, respectively, corresponding to a 0.1% mass loss from the baseline. With degraded

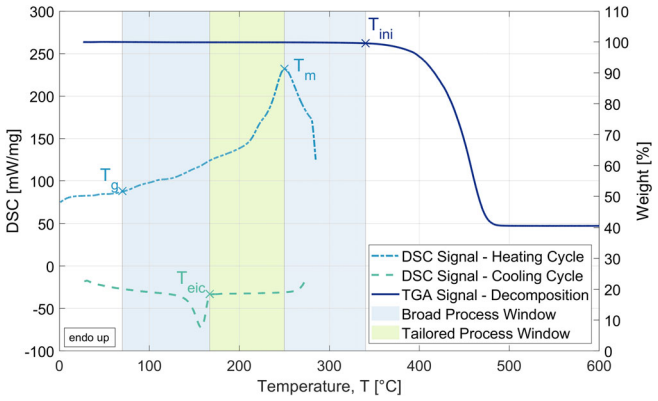

FIGURE 2 Definition of the overall process window, with the broad process window spanning T_g to T_{ini} and the tailored process window in the range T_{eic} to T_m for PA6 CF40

polymer exhibiting altered diffusion behavior,[25] T_{ini} allows judgment of the thermal stability of the given polymer.[65]

II. Lower limit: Chain motion is suppressed below the glass transition, T_g, and thus, it is the lowest temperature limit for bond formation to occur.[7,15,20] At T_g, the molecular chains become mobile, causing a sudden rise in heat capacity.[24,72] The longer a polymer is kept above T_g, the better the fusion bonding at the interlayer surface.[73] The glass transition is visible as change in heat capacity in differential scanning calorimetry (DSC).[72] Higher heating rates shift T_g to higher temperatures, with the shape depending on the previous cooling rate experienced by the polymer.[72]

2.6.2 | Tailored process window

III. Upper limit: A basic requirement in AM is that the extrusion temperature, T_{extr}, must be higher than the melting temperature, T_m. However, the substrate temperature, T_{sub}, must remain below T_{sub} to avoid polymer flow.[31,73] Therefore, the first hypothesis is that to optimize the mechanical properties and geometrical integrity, the upper limit of the tailored process window is $T_{sub} = T_m$.

IV. Lower limit: As crystallization may hinder bond formation,[15,17,32] the crystallization behavior when cooling from T_m to T_g is presumed to define the lower limit of the tailored process window. Crystallization can be analyzed in form of an exothermal peak in the cooling cycle of DSC measurements. The crystallization onset temperature, T_{ic}, indicates the first rise in crystallization rate and depends on the sensitivity of the measurement device.[74] The extrapolated onset temperature, T_{eic}, is regarded as the most relevant temperature for characterizing the onset of crystallization.[72] The second hypothesis is therefore that the lower limit of the crystallization is defined by the extrapolated onset of crystallization, which concludes the process window as depicted in Figure 2.

3 | MATERIALS AND METHODS

The chosen polyamide for this study was Akromid B3 ICF40,[75] supplied by AKRO-PLASTIC GmbH, as it is commonly used for automotive structural injection-molded parts. The density of the composite polymer was calculated on the basis of the manufacturer's pvT-data as $\rho_{c,25°C} = 1.344$ and $\rho_{c,300°C} = 1.220$ g/cm^3 at 1 bar atmospheric pressure. Samples of the neat polymer were additionally used in both DSC and TGA measurements. All samples were dried according to the manufacturer's recommendation and reached a water content of 0.02% before being sealed airtight.

3.1 | Dynamic scanning calorimetry

3.1.1 | Method for standard heating rates

DSC measurements were performed on a Netzsch DSC 204 F1 Phoenix® system, calibrated at corresponding temperature ranges. Samples were sliced to 7.00 ± 0.25 mg and placed into aluminum pans. Measurements according to DIN EN ISO 11357[74] and DIN 51005[76] were repeated five times per setup with nitrogen supplied at 25 ml/min to avoid oxidation reactions. The program was set to heat from equilibrium at −40 to 250°C before cooling back down to −40°C, equilibrating for 5 min and heating back up to 250°C. The first cycle was used to erase the thermal history of the material and to then determine the characteristic properties of the polymer in the second heating scan.[72] The heating/cooling rates were chosen as the lowest possible, 3 K/min, 10 K/mins standard for determining T_m and 20 K/min for T_g.[72]

Method for elevated heating rates: A double furnace DSC LAB SYS-DSC 8500 system made by PerkinElmer, together with HyperDSC® equipment was used for DSC measurements at elevated heating and cooling rates. The heating rates were chosen according to real heating rates in the present extrusion process at low, medium, and high screw speeds: 264, 484, and 660 K/min. The cooling rate was set to the maximum possible at 80 K/min. The incongruence between the heating and cooling rates had to be tolerated for technical reasons. Calibration determined the unavoidable errors

of 0.65°C at 100 K/min and 5.39°C at 660 K/min. The errors for 80, 264, and 484 K/min were determined by linear progression and shifted the thermal events to higher temperatures during heating and to lower temperatures during cooling, which was later taken into account in the analysis of the results. To adapt to the different DSC instrument and the high heating rates, samples were prepared as discs of 14 ± 0.5 mg and nitrogen was provided at a rate of 20 ml/min. The temperature program started at −75°C and was heated to 285°C at 264 K/min, and to 300°C at 484 and 660 K/min, before cooling down with 80 K/min to 20°C. Measurements were repeated 3 times and only performed on the filled polymer.

3.2 | Thermogravimetric analysis

The primary objective of the TGA measurements was to determine the initial degradation temperature, T_{ini}, under consideration of kinetic modeling. Additionally, TGA measurements have been identified as a reliable method for FVC-determination by various studies.[77–80] Measurements at standard heating rates of 2, 5, 10, and 20 K/min, were based on DIN EN ISO 11358[81] and DIN 51006[70] and performed on a TGA 209 F1 Libra® made by NETZSCH, which was calibrated with indium, tin, bismuth, zinc, aluminum, and silver.

Residue was burned off the Al_2O_3 pans before weighing and adding the samples of 10.5 ± 0.5 mg. The furnace was purged with 25 ml/min of nitrogen at 25°C for 15 min before heating the samples to 800°C. After 10 min at 800°C, the purge gas was switched to 25 ml/min of oxygen and the samples heated to 950°C. The combination of both purge gases enabled separate analysis of the polymer decomposition and the fiber and char decomposition stages.[77] The char content of neat PA6 samples at high temperatures under oxygen atmosphere was determined and deducted from the reinforced samples measurements, thus additionally enabling accurate determination of the fiber mass fraction.

4 | RESULTS AND DISCUSSION

4.1 | Dynamic scanning calorimetry

Figure 3 presents the average heat flow of the measurements of PA6 CF40 for heating and cooling rates of 3, 10, and 20 K/min. The glass transition temperature, T_g, was determined for all measurements by the half-step/midpoint temperature method.[72] No T_g is apparent for both the filled PA6 and the neat PA6 at elevated heating rates. The five measurements of PA6 CF40 in the second heating cycle at 20 K/min in Figure 4 exemplify the agreement in the repeatability of the measurements as well as the relaxation peak resulting from stresses in the microstructure, followed by a baseline shift after the peak. The height and width of the relaxation peak, as exemplified in Figure 4, showed to be greater for higher heating rates and thus dominates the temperature range of the glass transition at higher heating rates, such that no clear T_g can be determined.

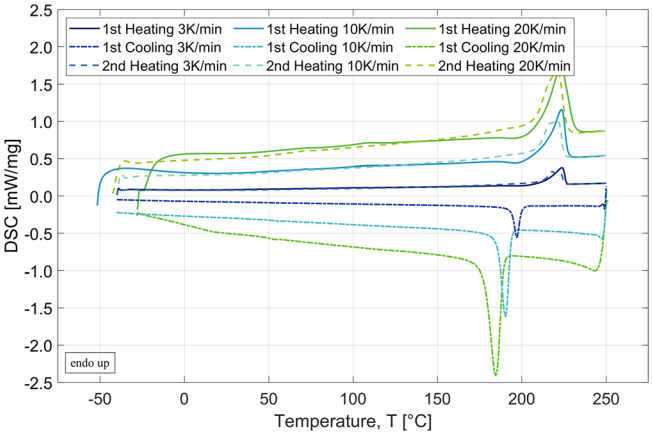

FIGURE 3 Average DSC measurements of PA6 CF40 at standard heating rates of 3, 10 K/min and 20 K/min

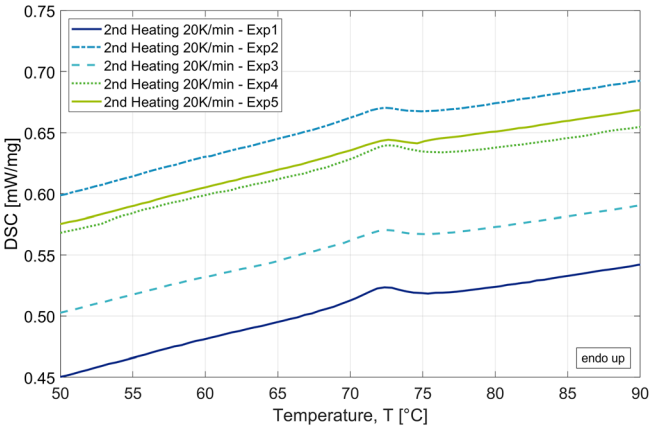

FIGURE 4 The glass transition of five measurements of PA6 CF40 in the second heating scan heated at 20 K/min

Table 1 presents the average T_g of the neat and filled material, showing that increasing heating rates shifted the glass transition to higher temperatures. As expected, a second heating scan showed no significant effect on the glass transition of the filled PA6.[56] The addition of fibers to the neat PA6 shifts the T_g to higher temperatures in the first heating scan. The baseline shift is more significant for the filled polymer as the fibers intensify the signal, and thus, no T_g was visible for the neat PA6 in the second heating scans.

For the presented additive manufacturing process the heating in the extrusion unit corresponds to the first heating cycle of the DSC measurements. As the process window is defined for the substrate temperature, which is reheated upon deposition of the new extrudate, the $T_{g,2}$ at the highest measurable heating rate of $T_g = 76°C$ was determined as lower limit for the broad processing window.

In the measurements of the melting point at elevated heating rates reached the maximum measurable signal of the machine, which reduced the analyzable sample size at the highest two heating rates. In future measurements choosing lower sample weights should prevent this problem. Table 2 presents the measured melting points for the filled and neat polymer. Greatly elevated heating rates shift the melting point to higher temperatures, while the second heating cycle, performed for the standard heating rates, shifted it to slightly lower temperatures as expected.[56] It is suggested that this results from the induced increase in crystallinity during controlled cooling in the first cycle. The addition of fibers to PA6 showed no significant change to the melting temperature at the standard heating rates.

Regarding the reheating of the substrate after deposition, the heating rates in real life were measured exemplary by insertion of thermocouples and showed to be significantly lower than in the extrusion unit itself. Therefore, the upper limit of the tailored processing window for T_{sub} is best represented by the standard heating rates of the second heating cycle and thus set to $T_m = 221°C$.

The literature suggests that higher cooling rates lead to a decrease in the crystallization temperature and a higher potential for cold crystallization.[51,72] Additionally, higher cooling rates lead to a lower degree of crystallinity, smaller crystal sizes, and larger amorphous domains, resulting in significantly higher interlaminar fracture toughness.[13,51] This decrease of crystallization temperature and extrapolated onset temperature, T_{eic}, is apparent across all heating rates and for both materials as presented in Table 3.

Although fibers are known to serve as nucleation sites and to increase the rate of nucleation,[25] the addition of fibers showed no significant influence on the characteristic crystallization temperatures, and the differences between filled and unfilled PA6 were in a comparable range to the standard deviations. The degree of crystallization is mostly dependent on the heating rates within the extrusion unit and the subsequent cooling rate after deposition. Therefore, the elevated heating rates must be considered for the process window definition. The largest restriction to the process window is given at 264 K/min for slow screw speed, and thus $T_{eic} = 166°C$ is suggested as the lower limit of the tailor process window.

4.2 | Thermogravimetric analysis

Figure 5 depicts the TGA results of PA6 CF40, while Figure 6 shows a comparison of filled and unfilled PA6 heated at 10 K/min. The mass change in a nitrogen atmosphere (<800°C) appeared to be a single-step mass loss, but the small shoulders in the rising edge of the DTG curves identify it as a two-step degradation process of the polymer. Purging the furnace with oxygen at 800°C leads to degradation of the carbon fibers in a third degradation step.

The slight decrease in mass of the neat PA6 between 100 and 250°C is assumed to be due to potential water

TABLE 1 Glass transition temperatures for the first and second heating scan of PA6 CF40 and the first heating scan of neat PA6 respectively for the standard heating rates

Heating rate [K/min]	$T_{g,1}$ [°C] PA6 CF40	$T_{g,2}$ [°C]	$T_{g,1}$ [°C] PA6
3	72 ± 0.6	73 ± 1.1	48 ± 0.4
10	74 ± 0.3	74 ± 0.2	54 ± 0.4
20	76 ± 0.6	75 ± 0.4	60 ± 0.2

TABLE 2 Melting temperatures for the first and second heating scans of PA6 CF40 and neat PA6

Heating rate [K/min]	$T_{m,1}$ [°C] PA6 CF40	$T_{m,2}$ [°C]	$T_{m,1}$ [°C] PA6	$T_{m,2}$ [°C]
3	224 ± 0.2	218 ± 0.6	225 ± 0.2	219 ± 0.0
10	224 ± 0.3	221 ± 0.3	225 ± 0.6	222 ± 0.2
20	224 ± 0.8	221 ± 0.2	226 ± 0.9	222 ± 0.5
264	253 ± 2.0	—	—	—
484	282 ± 3.5	—	—	—
660	278	—	—	—

TABLE 3 Extrapolated initial crystallization temperatures from the cooling scan of PA6 ICF40 and neat PA6

Heating rate [K/min]	Cooling rate [K/min]	T_{eic} [°C] PA6 CF40	T_{eic} [°C] PA6
3	3	200 ± 0.8	200 ± 0.0
10	10	194 ± 0.2	193 ± 0.3
20	20	189 ± 0.2	188 ± 0.3
264	80	166 ± 0.3	169 ± 1.1
484	80	159 ± 1.6	—
660	80	153 ± 0.3	—

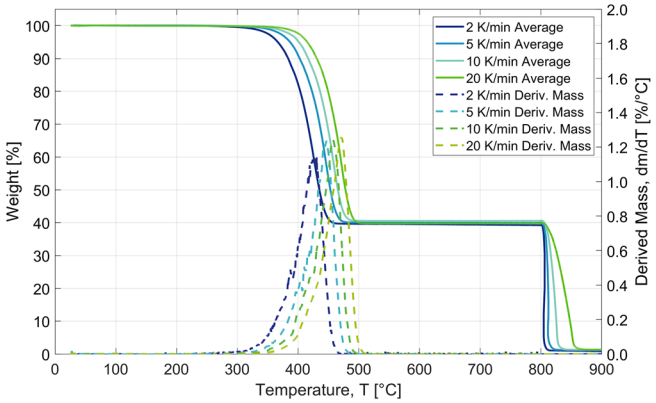

FIGURE 5 Degradation behavior of PA6 CF40 at heating rates of 2, 5, 10, and 20 K/min

intake as the samples were tested at a later point in time. The mass loss in the neat PA6 sample under nitrogen is calculated using DIN 11358:[81]

$$M_L = \left(\frac{m_s - m_c}{m_s}\right) \cdot 100\% \tag{8}$$

where m_s is the composite weight after water evaporation and before degradation, and m_c is the weight of the remaining char. If m_c is replaced by m_f for the remaining mass of fibers and char, the residual weight of the filled sample can be determined, with the results presented in Table 4. As expected, the variation in heating rates produced no significant difference in mass loss. The remaining char content, m_c, of the neat PA6 sample in inert gas was deducted from the fiber contents of all measurements for the corrected fiber content. The char content of the neat resin samples must also be deducted, as the same residual weight fraction of additives will remain in the filled samples after polymer degradation under nitrogen purge gas. The average of this corrected fiber content produced a fiber mass fraction of 39.4% with a standard deviation of 0.4%.

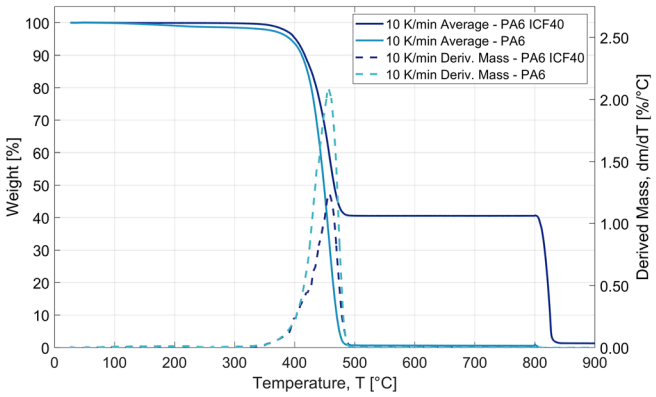

FIGURE 6 Average mass loss in the degradation process at 10 K/min of PA6 CF40 and neat PA6

The initial degradation temperatures at 0.1% mass loss range from 308°C at 2 K/min to 336°C at 20 K/min, with standard deviations of 0.1 and 1.7°C, respectively, with completed degradation at T_{fin} of 511 and 503°C, respectively, with standard deviations of 0.5 and 1.6°C. The difference between T_{ini} at 2 K/min and at 20 K/min is therefore 28°C and for T_{fin} only 8°C. The significantly smaller difference in the final degradation temperatures suggests a low thermal inertia of the system.

The model-free approach to degeneration kinetics by Friedman[66] was used to determine the degradation behavior within the extrusion unit, and additionally for the case of subsequent hot gas heating of the substrate for long layer times. The model is based on measurements under nitrogen atmosphere and only predicts the degradation of the polymers, as the fibers degrade at temperatures significantly higher than the processing temperatures.

Smoothing of the data alters the mass loss by a maximum of 0.01% while achieving a steadier modeling basis, for which the Friedman model achieves a satisfactory fit of $R^2 = 0.99992$. Based on the kinetic model, the dynamic degradation behavior can be presented graphically as shown in Figure 7, with T_{ini} shifting to higher temperatures for increasing heating rates.

Figure 8 presents the Friedman plot of $log(dx/dt)$ over the inverse temperature. The gradient of the isoconversional lines corresponds to $E(\alpha)/RT$, with the universal gas constant R = 1.987 cal/Kmol and the current temperature T. At high temperatures (low conversions), the isoconversional lines lie almost on top of each other, implying a process close to the first order.[82] They can be used to calculate the required activation energy $E(\alpha)$ as a function of the degree of conversion α, as shown in Figure 9 for the entire thermal decomposition. Although this has no direct effect on the process window, it can later be used for the calculation of required heat

TABLE 4 Average mass contents in nitrogen atmosphere with m_s at 300°C, $m_{c/f}$ at 600°c and m_{O_2} in oxygen at 900°c with corresponding mass losses under nitrogen $M_{L,1}$ and the overall mass loss under combined atmospheres $M_{L,2}$

Heating rate [K/min]		$m_{s/f,Avg}$ [%]	$m_{c/f,Avg}$ [%]	$m_{O_2,Avg}$ [%]	$M_{L,1,Avg}$ [%]	$M_{L,2,Avg}$ [%]
PA6	10	98.5 ± 0.0	0.6 ± 0.1	−0.1 ± 0.1	99.4 ± 0.1	100.1 ± 0.1
PA6 CF40	2	99.5 ± 0.2	39.5 ± 0.4	0.9 ± 0.2	60.3 ± 0.3	99.1 ± 0.2
	5	99.8 ± 0.0	40.0 ± 0.1	1.2 ± 0.1	59.9 ± 0.1	98.8 ± 0.1
	10	99.8 ± 0.0	40.5 ± 0.2	1.3 ± 0.1	59.4 ± 0.2	98.7 ± 0.1
	20	99.8 ± 0.3	39.7 ± 0.3	1.3 ± 0.1	60.2 ± 0.3	98.7 ± 0.1

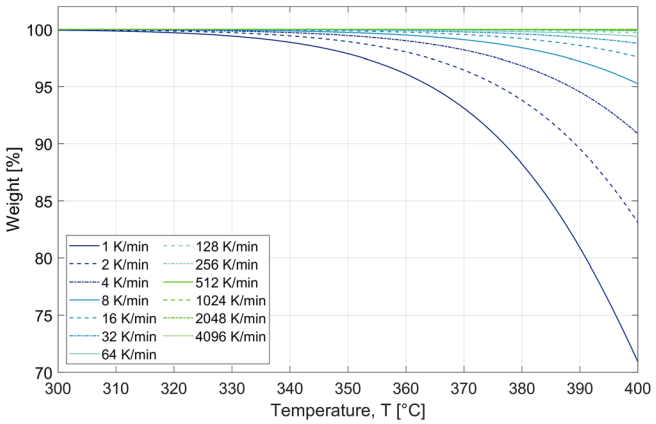

FIGURE 7 Predicted mass loss for heating rates of up to 4096 K/min, determined by the isoconversional Friedman method

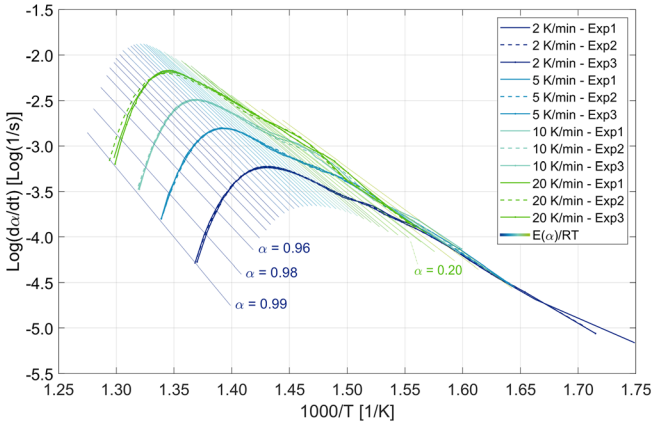

FIGURE 8 Friedman plot showing the $log(dx/dt)$ over the inverse of the temperature with the corresponding isoconversional lines for the determination of the activation energy

input for potential reheating. Figure 9 also illustrates and confirms the two stages of the thermal degradation process with a stage change close to 0.2.

This model was used to model a multistep prediction of the degradation behavior throughout the entire extrusion process. Therefore, the temperature program was adapted to drying for 4 h at 80°C, cooling down during the transfer to the extrusion system, rapid heating at the maximum 660 K/min, followed by ballistic cooling to room temperature. Figure 10 presents the temperature program and the corresponding degradation which reached 0.01% until deposition. This confirmed that the decisive factor for the degradation is in fact the heating rate in the extrusion unit. According to the results presented in Figures 7, 0.1% degradation occurs at 367°C for a heating rate of 64 K/min, at 379°C for a heating rate of 128 K/min and < 400°C for heating at 512 K/min. With heating rates of 200 to 700 K/min in the extrusion unit, the maximum degradation is expected for the lowest heating rate.

Sonmez and Hahn[83] suggested in their study of PEEK that the maximum tolerable weight loss during tape placement is in fact 0.01%, which would shift the initial degradation temperature T_{ini} to lower temperatures.

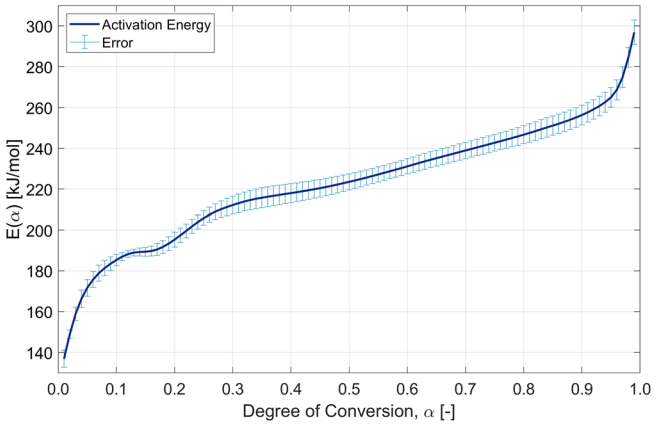

FIGURE 9 Predicted activation energy $E(\alpha)$ in relation to the degree of conversion α

For the slowest heating rate above, 64 K/min this shifts $T_{ini,0.01\%}$ to 330°C, which is still well above any processing temperatures and represents a conservative limit for the degradation process.

From the knowledge of a two-step degradation process under nitrogen, as presented in Figure 8 and

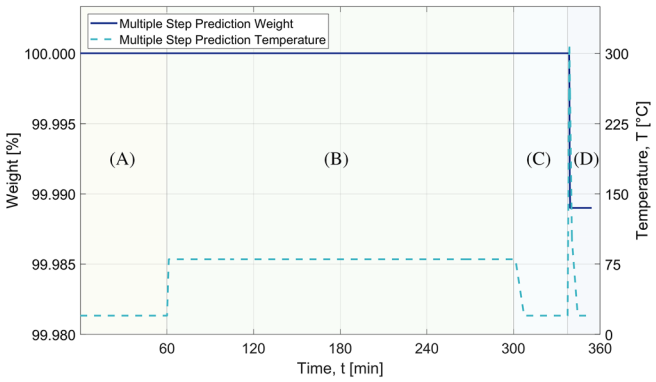

FIGURE 10 Multiple-step prediction of the current extrusion process with the corresponding degradation of PA6 CF40 during (A) storage, (B) drying at 80°C for 4 h, (C) conveying to the unit, and (D) the extrusion process

Figure 9, a model-based approach was conducted to verify the Friedman model. The model-based calculations yielded a fit of $R^2 = 0.99992$ and aligned very closely with the results of the model-free approach.

$$V_f = \psi \cdot \frac{\rho_c}{\rho_f} = \frac{m_f}{m_c} \cdot \frac{\rho_c}{\rho_f} \cdot 100\% \tag{9}$$

In addition, the calculated fiber mass fraction was used to calculate the actual fiber volume fraction, as important parameter in composite design:

Where ϕ is the fiber mass fraction of 39.4%, and ρ_c and ρ_f are the composite and fiber densities. Equation (9) therefore yields a fiber volume fraction of $V_f = 26.9\%$, taking into account the deduction of the char residue contents determined in the nitrogen atmosphere for the neat PA6 samples, which can result from additives applied during compounding.[72] The remaining low char content of the filled samples may correspond to small amount of carbonaceous material, which did not decompose into smaller volatile components and thus remained visible in the measurement even at high temperatures under an oxidizing atmosphere.

The interpretation of the results considers that the measurements were performed under nitrogen atmosphere, while the real-world process operates under the influence of oxygen. The scope of this study allowed single comparable measurements to be made under oxygen atmosphere (20% O_2 and 80% N_2) for both PA6 CF40 and neat PA6. The results showed no significant difference in the respective initial degradation temperatures and therefore the authors presume a high degree of reliability for the determined degradation behavior. While not relevant to the process window, the use of oxygen as purge gas showed noteworthy changes in the degradation behavior of the carbon fibers at temperatures above 450°C, as was expected. No pressures were considered in the above measurements and thus no conclusion can be drawn regarding the precise degradation behavior under elevated pressures. This was found to be tolerable for this study, as the pressures in the extrusion unit for EAM are significantly lower than the pressures in, for example, injection molding.

Kinetic modeling enabled the prediction of the degradation behavior beyond the measurable range. Smoothing of the raw data for the calibration of the Friedman model had little effect on the curve characteristics but enabled modeling with a good agreement of data and model. It would also have been possible to use other model-free methods, such as Flynn-Wall-Ozawa (FWO) or Kissinger-Akahira-Sunose (KAS).[65] Nonetheless, based on the broad consensus among the aims of the Friedman method and the present part of this study, as well as the coherence with the model-based approach used, the Friedman method represents a satisfactory representation of the data and allows for the deduction of all relevant variables.

4.3 | Validation

Various methods exist for analyzing the layer interface of additively manufactured parts. For the requirements of this study, a three-point bending test according to DIN EN ISO 178 was conducted. Compared to conventional 3D printing, the test specimens were not individually printed but milled from larger parts that resemble the real EAM process and were manufactured with realistic layer times and substrate temperatures. To avoid disturbance factors, such as, the influence of different screw speeds and traversing speeds, these were kept constant and the different layer durations were realized by a holding position outside the component geometry.

The range of substrate temperatures at which components can still be manufactured appeared to be limited in both directions. The upper limit corresponded quite well with the melt temperature at T_m°=°221°C, as parts appeared to be slightly too hot, risking the structural integrity, and prohibiting a uniform build-up. Manufacturing parts at substrate temperatures below the glass transition around 75°C was also unfeasible, as the parts delaminated during removal from the build platform. Based on these findings, parts were produced with substrate temperatures in the producible range between 75 and 210°C, which corresponded to layer times between 80 and 12 s. To confirm the hypothesis of good interlayer bond formation between T_{eic} and T_m, components were subsequently tested by a 3-point bending test. Eight samples of each setup were tested with 5 N

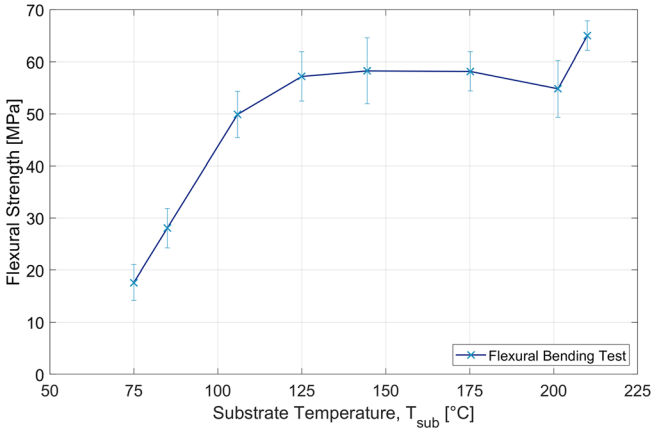

FIGURE 11 3-point bending results for specimens manufactured with different substrate temperatures by varying layer times

preload at testing speeds of 2 mm/min, with the results presented in Figure 11.

Contrary to expectations, the results show no decrease in bond strength for substrate temperatures below the extrapolated onset of crystallization at T_{eic}°=°166°C. The decrease in flexural strength only appears for parts of substrate temperatures below 125°C. The reason for this may be that crystallization is not only temperature-controlled but also time-controlled.[32] Depending on the cooling rate, it is therefore possible that the next layer is deposited before nucleation is completed and thus bond formation can occur before crystallization is complete.

In addition to the substrate temperature, the resulting interface temperature is particularly relevant for adhesion formation. Assuming that only amorphous material is present and simplifying that the heat capacity remains constant over the entire temperature range, the interface temperature T_{int} can be estimated using the following equation:[31]

$$T_{int} = (T_1 + T_2)/2 \tag{10}$$

The temperatures T_1 and T_2 are the substrate temperature and the extrudate temperature of the new layer, respectively. With the critical substrate temperature of 125°C and an extrusion temperature of 280°C the critical interface temperature is calculated at 202°C. A comparison with the DSC results of section 4.1 show that this is just below the onset melt temperature. This means that at substrate temperatures below 125°C, the interface is not sufficiently heated by the subsequent layer to achieve the required chain mobility of the melt, which reduces the strength of the manufactured part. This was verified by imprinting of thermocouples into parts of identical substrate temperatures, which showed high coherence to the approximation through Equation (10).

Furthermore, the degree of bond was calculated according to Equation (1), based on the method presented by Consul et al[45] for semicrystalline PAEK. Results showed that the degree of bond reaches 1 considerably fast, supporting the above suggestion, that the most significant aspect is whether the interface reaches the onset of melt for sufficient chain mobility.

5 | CONCLUSION

Fusion bonding has proven to be a significant factor for mechanical performance of additively manufactured parts. Due to complex thermal and mechanical behavior, the process windows for materials and AM processes are often determined by extensive experimental investigations, which are costly and time-consuming. In this work, a thermal analysis approach was followed to determine the process window for semicrystalline polymers. This allowed a separate definition of a feasible process window, in which fusion bonding could generally occur, as well as an optimized process window in which satisfactory bond strength can be expected. These process windows were explicitly defined for the substrate temperature, as this can be easily determined through noncontact measurements in any extrusion-based AM process.

Dynamic scanning calorimetry (DSC) enabled the determination of T_g, T_m, and T_{eic} and contributed to an understanding of the influence of heating rates, fiber addition, and the complex interaction between endothermal and exothermal processes. Degradation behavior was analyzed by dynamic measurements in thermogravimetric analysis. The application of the Friedman method established a quantitative framework with which to determine the initial degradation temperature T_{ini} at heating rates outside of the measurable range. It also enhanced understanding of the decomposition behavior during the printing process itself. The proposed process windows resulting from the thermal analyses were validated by three-point bending tests of specimens manufactured at different layer times and consequently different substrate temperatures.

The first hypothesis of a broad processing window was confirmed as the range between T_g and T_{ini} in which the molecular chains are mobile enough that fusion bonding can generally occur without degradation taking place. The experimental results also confirmed that the upper limit of the optimized processing window, namely, the melting point, is also the upper limit to the manufacturability with a part's integrity in danger for substrate temperatures higher than T_m. The lower limit of the optimal process window was suggested to be the onset of crystallization as it may prevent bond formation. This hypothesis,

however, had to be refuted as experimental results showed to provide sufficient bond strength for even lower substrate temperatures. It is therefore proposed to set the lower limit to the lowest substrate temperature at which the combined interface temperature still exceeds the onset of melt, thus allowing for sufficient chain mobility for fusion bonding.

The presented approach represents a highly effective shortcut for the determination of ideal process parameters in both industrial and scientific additive manufacturing processes. Especially for applications where high manufacturing flexibility must be achieved in a short time with limited resources, this approach can significantly increase the efficiency of parameter determination for semi-crystalline polymers. With the elimination of extensive experimentation on printed parts, the approach also becomes advantageous from a sustainability perspective. The thermal analyses only require small quantities in the gram range, while experimental mechanical determination requires a high material input as well as long printing and testing times.

The molecular weight distribution, as well as the time component of intimate contact and fusion bonding are not considered. While the process window is defined for the average molecular weight of the polymer, longer chains may already crystallize at higher temperatures.[17] However, since T_{eic} was found to be less influential in fusion bonding than expected, this should only have a minimal impact. At the same time, the time component in both intimate contact and fusion bonding plays a critical role in bond strength development[32] and thus poses potential for further research.

Further research is also suggested on the effect of cooling and heating of the substrate. This would allow shorter or longer layer times, however, the effect on the mechanical properties, specifically the degree of bond, require further investigation. With fibers primarily orientated along the strand direction in the x-y-plane,[84,85] the fiber orientation itself is disregarded for thermal and mechanical analyses of interface properties and bond strength in the out of plane direction.

ACKNOWLEDGMENTS

This research was supported by the BMW Group and the Chair of Carbon Composites at the Technical University of Munich. The authors express their appreciation to Johannes Roth for his assistance in sample preparation and DSC analysis at the BMW Group. We would also like to thank AKRO-PLASTIC GmbH for providing polymer samples for this study. This research did not receive any specific grant from funding agencies in the public, commercial, or not-for-profit sectors.

Open access funding enabled and organized by Projekt DEAL.

ORCID

Nevine Tagscherer https://orcid.org/0000-0003-3782-6212
Patrick Consul https://orcid.org/0000-0002-2972-7735

REFERENCES

[1] E. Barnett, C. Gosselin, *Addit. Manuf.* **2015**, *7*, 27.
[2] J. Tierney, J. W. Gillespie, *J. Compos. Mater.* **2003**, *37*, 1745.
[3] S. Ford, M. Despeisse, *J. Cleaner Prod.* **2016**, *137*, 1573.
[4] DIN Deutsches Institut für Normung e. V, *Additive manufacturing – General principles – Part 2: Overview of process categories and feedstock*, Beuth Verlag GmbH, Berlin **2016**.
[5] DIN Deutsches Institut für Normung e. V, *Additive manufacturing - Standard specification for material extrusion based additive manufacturing of plastic materials - Part 2: Process - Equipment*, Beuth Verlag GmbH, Berlin **2018**.
[6] C. E. Duty, V. Kunc, B. Compton, B. Post, D. Erdman, R. J. Smith, R. Lind, P. Lloyd, L. J. Love, *Rapid Prototyping J.* **2017**, *23*, 181.
[7] V. Kishore, C. Ajinjeru, A. Nycz, B. Post, J. Lindahl, V. Kunc, C. E. Duty, *Addit. Manuf.* **2017**, *14*, 7.
[8] J. Go, A. J. Hart, *Addit. Manuf.* **2017**, *18*, 276.
[9] C. Bellehumeur, L. Li, Q. Sun, P. Gu, *J. Manuf. Processes* **2004**, *6*, 170.
[10] C. B. Sweeney, B. A. Lackey, M. J. Pospisil, T. C. Achee, V. K. Hicks, A. G. Moran, B. R. Teipel, M. A. Saed, M. J. Green, *Sci. Adv.* **2017**, *3*, e1700262.
[11] S.-H. Ahn, M. Montero, D. Odell, S. Roundy, P. K. Wright, *Rapid Prototyping J.* **2002**, *8*, 248.
[12] F. Yang, R. Pitchumani, *Macromolecules* **2002**, *35*, 3213.
[13] S. C. Malguarnera, A. Manisali, *Polym. Eng. Sci.* **1981**, *21*, 586.
[14] Y.-Q. Xue, T. A. Tervoort, P. J. Lemstra, *Macromolecules* **1998**, *31*, 3075.
[15] C. M. Stokes-Griffin, P. Compston, *Compos. Part A: Appl. Sci. Manuf.* **2016**, *84*, 17.
[16] D. Grewell, A. Benatar, *IPP* **2007**, *22*, 43.
[17] S. Padaki, L. T. Drzal, *Compos. Interfaces* **1996**, *4*, 133.
[18] J. Schell, J. Guilleminot, C. Binetruy, P. Krawczak, *J. Mater. Process. Technol.* **2009**, *209*, 5211.
[19] C.-W. Tsao, D. L. DeVoe, *Microfluid. Nanofluid.* **2009**, *6*, 1.
[20] F. O. Sonmez, H. T. Hahn, *J. Thermoplast. Compos. Mater.* **1997**, *10*, 543.
[21] D. Cavallo, L. Gardella, G. C. Alfonso, G. Portale, L. Balzano, R. Androsch, *Colloid Polym. Sci.* **2011**, *289*, 1073.
[22] Y. Amintowlieh, A. Sardashti, L. C. Simon, *Polym. Compos.* **2012**, *33*, 985.
[23] NETZSCH-Gerätebau GmbH, Thermal Properties of Polymers Version 3.0.
[24] M. Bonnet, *Werkstoffauswahl und Fallbeispiele*, Springer Fachmedien Wiesbaden, Wiesbaden **2016**.
[25] N. Boyard Ed., *Heat transfer in polymer composite materials: Forming processes*, Wiley-ISTE, London **2016**.
[26] L. J. Love, V. Kunc, O. Rios, C. E. Duty, A. M. Elliott, B. K. Post, R. J. Smith, C. A. Blue, *J. Mater. Res.* **2014**, *29*, 1893.
[27] V. K. Stokes, *Polym. Eng. Sci.* **1989**, *29*, 1310.
[28] B. N. Turner, R. Strong, S. A. Gold, *Rapid Prototyping J.* **2014**, *20*, 192.
[29] C. Ajinjeru, V. Kishore, J. Lindahl, Z. Sudbury, A. A. Hassen, B. Post, L. Love, V. Kunc, C. Duty, *Int. J. Adv. Manuf. Technol.* **2018**, *99*, 411.

[30] Q. Sun, G. M. Rizvi, C. T. Bellehumeur, P. Gu, *Rapid Prototyping J.* **2008**, *14*, 72.
[31] C. J. G. Plummer, P.-E. Bourban, J.-E. Zanetto, G. D. Smith, J.-A. E. Månson, *J. Appl. Polym. Sci.* **2003**, *87*, 1267.
[32] C. A. Butler, R. L. Mccullough, R. Pitchumani, J. W. Gillespie, *J. Thermoplast. Compos. Mater.* **1998**, *11*, 338.
[33] D. Slotfeldt-Ellingsen, E. Magnus, E. Ekern, E. Holtmon, L. Corneliussen, *Polym. Compos.* **1986**, *7*, 431.
[34] G. D. Smith, C. J. Plummer, P.-E. Bourban, J.-A. E. Månson, *Polymer* **2001**, *42*, 6247.
[35] O. A. Ezekoye, C. D. Lowman, M. T. Fahey, A. G. Hulme-Lowe, *Polym. Eng. Sci.* **1998**, *38*, 976.
[36] P. H. Dara, A. C. Loos, *Thermoplastic matrix composite processing model*, Hampton, VA **1985**.
[37] W. I. Lee, G. S. Springer, *J. Compos. Mater.* **1987**, *21*, 1017.
[38] R. P. Wool, B.-L. Yuan, O. J. McGarel, *Polym. Eng. Sci.* **1989**, *29*, 1340.
[39] S. C. Mantell, G. S. Springer, *J. Compos. Mater.* **1992**, *26*, 2348.
[40] R. Pitchumani, S. Ranganathan, R. C. Don, J. W. Gillespie, M. A. Lamontia, *Int. J. Heat Mass Transfer* **1996**, *39*, 1883.
[41] B. B. Sauer, W. G. Kampert, M. D. Wakeman, S. Yuan, *Compos. Sci. Technol.* **2016**, *129*, 166.
[42] F. Yang, R. Pitchumani, *J. Mater. Sci.* **2001**, *36*, 4661.
[43] F. Yang, R. Pitchumani, *Polym. Compos.* **2003**, *24*, 263.
[44] Y. H. Kim, R. P. Wool, *Macromolecules* **1983**, *16*, 1115.
[45] P. Consul, A. Chaplin, N. Tagscherer, S. Zaremba, K. Drechsler, *Polym. Int.* **2020**, *70*, 1099.
[46] P. G. D. Gennes, L. Leger, *Annu. Rev. Phys. Chem.* **1982**, *33*, 49.
[47] C. Ageorges, L. Ye, M. Hou, *Compos. Part A: Appl. Sci. Manuf.* **2001**, *32*, 839.
[48] G. Regnier, C. Nicodeau, J. Verdu, Cinquin, Jacques, F. Chinesta, in Japan Society for Composite Materials (Hg.) 2007 – 16th International Conference on Composite, Vol. 16, p. 1.
[49] W. Weng, G. Chen, D. Wu, *Polymer* **2003**, *44*, 8119.
[50] DIN Deutsches Institut für Normung e. V., DIN EN ISO 11357-7:2015, Plastics - Differential scanning calorimetry (DSC) - Part 7: Determination of crystallization kinetics, Beuth Verlag GmbH, Berlin, 83.080.01 **2015**.
[51] W. Dietz, *Colloid Polym. Sci.* **1981**, *259*, 413.
[52] T. Ozawa, *Polymer* **1971**, *12*, 150.
[53] T. Guglhör, M. Korkisch, M. Sause, 20th International Conference on Composite Materials **2015**.
[54] D. Mileva, A. Monami, D. Cavallo, G. C. Alfonso, G. Portale, R. Androsch, *Macromol. Mater. Eng.* **2013**, *298*, 938.
[55] D. Mileva, I. Kolesov, R. Androsch, *Colloid Polym. Sci.* **2012**, *290*, 971.
[56] F. Parres, J. E. Crespo, A. Nadal-Gisbert, *J. Appl. Polym. Sci.* **2009**, *114*, 713.
[57] M. Ito, K. Mizuochi, T. Kanamoto, *Polymer* **1998**, *39*, 4593.
[58] L. Lin, A. S. Argon, *Macromolecules* **1994**, *27*, 6903.
[59] H. Quan, Z.-M. Li, M.-B. Yang, R. Huang, *Compos. Sci. Technol.* **2005**, *65*, 999.
[60] M. Run, H. Song, C. Yao, Y. Wang, *J. Appl. Polym. Sci.* **2007**, *106*, 868.
[61] E. Boucher, J. P. Folkers, C. Creton, H. Hervet, L. Léger, *Macromolecules* **1997**, *30*, 2102.
[62] J.-E. Zanetto, C. J. G. Plummer, P.-E. Bourban, J.-A. E. Månson, *Polym. Eng. Sci.* **2001**, *41*, 890.
[63] P. Šimon, *J. Therm. Anal. Calorim.* **2004**, *76*, 123.
[64] E. Moukhina, *J. Therm. Anal. Calorim.* **2012**, *109*, 1203.
[65] R. Balart, D. Garcia-Sanoguera, L. Quiles-Carrillo, N. Montanes, S. Torres-Giner, *Polymer* **2019**, *11*, 11.
[66] H. L. Friedman, *J. Polym. Sci., C Polym. Symp.* **1964**, *6*, 183.
[67] S. Habibu, N. M. Sarih, N. A. Sairi, M. Zulkifli, *R. Soc. Open Sci.* **2019**, *6*, 190869.
[68] P. Tranchard, S. Duquesne, F. Samyn, B. Estèbe, S. Bourbigot, *J. Anal. Appl. Pyrolysis* **2017**, *126*, 14.
[69] C. Ajinjeru, V. Kishore, T. Z. Sudbury, C. E. Duty, J. Lindahl, A. A. Hassen, B. Post, L. J. Love, V. Kunc, SAMPE 2017 - Seattle, WA **2017**.
[70] DIN Deutsches Institut für Normung e. V., Thermal analysis (TA) - Thermogravimetry (TG) - Principles, Beuth Verlag GmbH, Berlin, ICS 71.040.40 **2005**.
[71] ASTM International, Standard Test Method for Thermal Stability by Thermogravimetry, ASTM International, West Conshohocken, PA, 17.200.99.
[72] G. W. Ehrenstein, G. Riedel, P. Trawiel, *Thermal analysis of plastics: Theory and practice*, Carl Hanser Verlag, Munich **2004**.
[73] R. B. Dinwiddie, V. Kunc, J. M. Lindal, B. Post, R. J. Smith, L. J. Love, C. E. Duty, in *Thermosense: Thermal Infrared Applications XXXVI* (Ed: F. P. Colbert) SPIE Sensing Technology + Applications, United States **2014**.
[74] DIN Deutsches Institut für Normung e. V., DIN EN ISO 11357-1:2017–02, Plastics - Differential scanning calorimetry (DSC) - Part 1: General principles, Beuth Verlag GmbH, Berlin, 83.080.01 **2017**.
[75] AKRO-PLASTIC GmbH, AKROMID® ICF (PA 6, PA 6.6, PPA), AKROTEK® ICF (Aliphatisches Polyketon), AKROLOY® ICF (PA-Blend): Kohlenstofffaserverstärkte Compounds
[76] DIN Deutsches Institut für Normung e. V., DIN 51005:2019–06, Thermal analysis (TA) - Vocabulary, Beuth Verlag GmbH, Berlin **2019**.
[77] D. Grund, M. Orlishausen, I. Taha, *Polym. Test.* **2019**, *75*, 358.
[78] Q. Wang, H. Ning, U. Vaidya, S. Pillay, L.-A. Nolen, *Compos. Part A: Appl. Sci. Manuf.* **2015**, *73*, 80.
[79] Y. Kim, C. Choi, S. K. S. Kumar, C.-G. Kim, S.-W. Kim, J. H. Lim, *Compos. Part A: Appl. Sci. Manuf.* **2017**, *102*, 40.
[80] R. Y. Yee, T. S. Stephens, *Thermochim. Acta* **1996**, *272*, 191.
[81] DIN Deutsches Institut für Normung e. V., DIN EN ISO 11358-1:2014–10, Plastics – Thermogravimetry (TG) of polymers – Part 1: General principles, Beuth Verlag GmbH, Berlin, 83.080.01 **2014**.
[82] P. R. Hondred, S. Yoon, N. Bowler, E. Moukhina, M. R. Kessler, *High Perform. Polym.* **2011**, *23*, 335.
[83] F. O. Sonmez, H. T. Hahn, *J. Thermoplast. Compos. Mater.* **1997**, *10*, 198.
[84] J. Wang, J. F. O'Gara, C. L. Tucker, *J. Rheol.* **2008**, *52*, 1179.
[85] B. P. Heller, D. E. Smith, D. A. Jack, *Addit. Manuf.* **2016**, *12*, 252.

How to cite this article: N. Tagscherer, P. Consul, I. L. Kottenstedde, H. Latiri, S. Zaremba, K. Drechsler, *Polym. Compos.* **2021**, *42*(10), 5209. https://doi.org/10.1002/pc.26216